Volume 5 | Number 5 | May 2017 | Pages 863–1064

Biomaterials Science

rsc.li/biomaterials-science

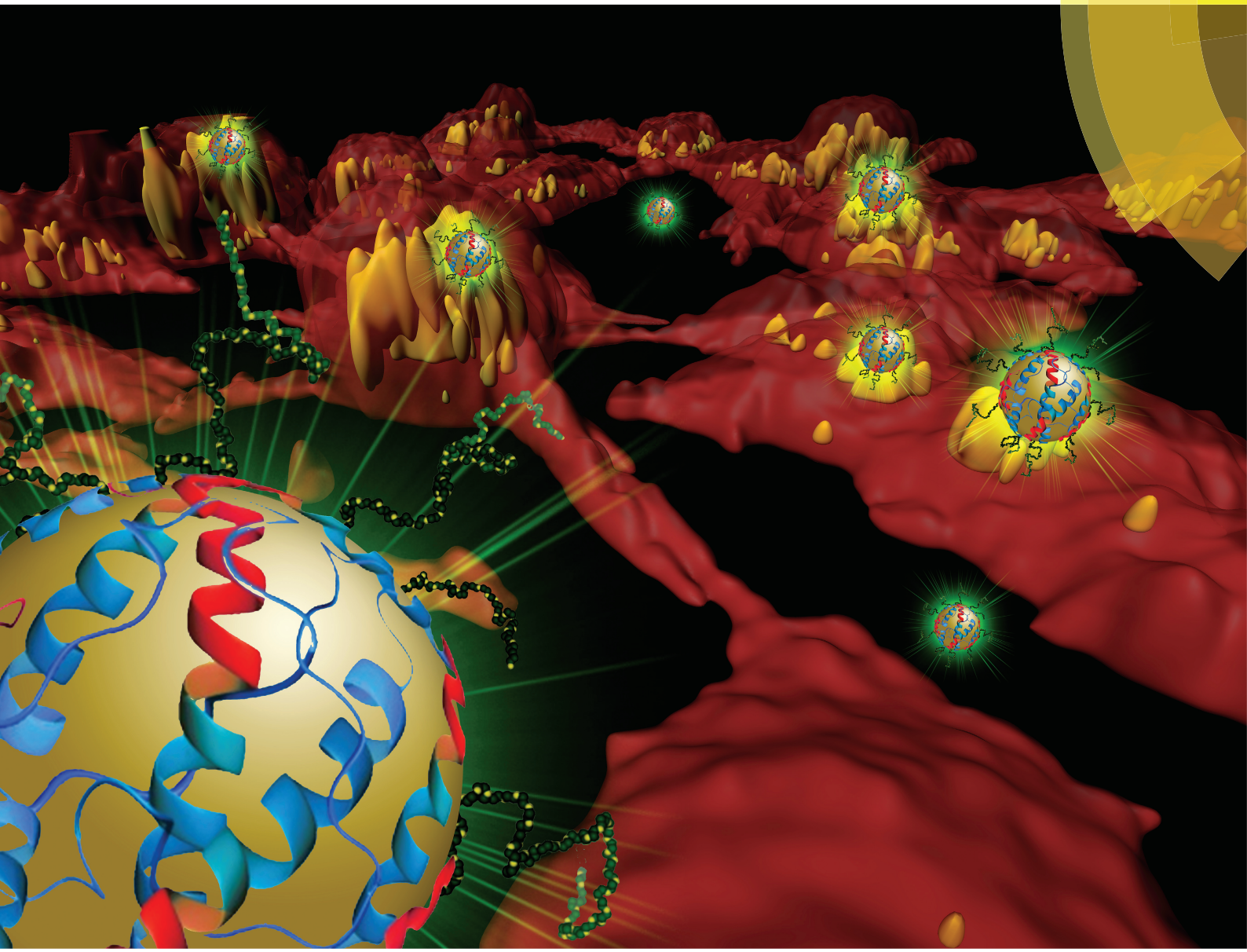

ISSN 2047-4849

ROYAL SOCIETY OF CHEMISTRY

COMMUNICATION

Tanja Weil *et al.*

NIR-emitting and photo-thermal active nanogold as mitochondria-specific probes

Biomaterials Science

COMMUNICATION

View Article Online
View Journal | View Issue

Cite this: *Biomater. Sci.*, 2017, **5**, 966

Received 28th December 2016,
Accepted 28th February 2017

DOI: 10.1039/c6bm00951d

rsc.li/biomaterials-science

NIR-emitting and photo-thermal active nanogold as mitochondria-specific probes†

Sabyasachi Chakrabortty,[a,b] Miguel Sison,[c] Yuzhou Wu,[a,b] Anita Ladenburger,[d] Goutam Pramanik,[a] Johannes Biskupek,[d] Jerome Extermann,[c,e] Ute Kaiser,[d] Theo Lasser[c] and Tanja Weil*[a,b]

We report a bioinspired multifunctional albumin derived polypeptide coating comprising grafted poly(ethylene oxide) chains, multiple copies of the HIV TAT derived peptide enabling cellular uptake as well as mitochondria targeting triphenyl-phosphonium (TPP) groups. Exploring these polypeptide copolymers for passivating gold nanoparticles (Au NPs) yielded (i) NIR-emitting markers in confocal microscopy and (ii) photo-thermal active probes in optical coherence microscopy. We demonstrate the great potential of such multifunctional protein-derived biopolymer coatings for efficiently directing Au NP into cells and to subcellular targets to ultimately probe important cellular processes such as mitochondria dynamics and vitality inside living cells.

Cell organelle-specific bio-imaging tools, diagnostics and therapeutics have emerged as important strategies in recent biomedical research.[1] In drug delivery, subcellular targeting offers great prospects to enhance the effect of drug molecules by directed transport to the targeted organelles and potentially minimized side effects as compared to non-directional cellular targeting.[1] Live cell imaging with nanoparticles that selectively target specific intracellular organelles reveals increased spatial and temporal resolution with greatly decreased acquisition time per pixel allowing visualization of *e.g.* intracellular particle distributions for specific subcellular organelles. To date, a number of sub-cellular compartments such as the plasma membrane,[2] endosomes,[3] Golgi complex,[4] cytosol,[5] mitochondria[6] or nucleus[7] have been targeted. Addressing mitochondria is of particular interest as they are indispensable for providing energy to eukaryotic cells and control apoptosis (programmed cell death),[8] making them an important therapeutic target.

High-speed Raman microscopy,[9] super-resolution STED microscopy[10] as well as optical coherence microscopy (OCM)[11–13] offer three-dimensional live cell imaging with the highest resolution and fast response times. However, identification of the optimal imaging probes providing efficient cellular uptake, significant photo-stability, and low cellular toxicity is essential. Furthermore, escape from the endosome and subcellular organelle targeting remains critical for various studies inside living cells.[14] Gold nanoparticles (Au NPs) provide many attractive features for cellular imaging. They exhibit fluorescence at sizes below 2 nm and reveal NIR emission (NIR-Au), which is well-suited for less invasive cellular and tissue imaging.[15] In addition, they are resistant to photobleaching under continuous illumination[16] and they are considered more bio-compatible than other metals. Alternatively, larger, non-fluorescent Au NPs offer plasmonic features, which can be exploited for OCM.[13] They serve as localized "heating zones" and as thermally driven phase objects with an increased cross-section making them suitable as efficient photo-thermal contrast agents.[13] Both NIR-Au[17–21] and larger Au NPs have been successfully synthesized before and were mainly applied as drug delivery vehicles because of their high payloads, localized mechanical damage and improved photo thermal therapy applications.[22] However, efforts to identify Au NPs as probes for observing the dynamics of a particular organelle inside a living cell for prolonged periods still remains critical, where subcellular targeting capabilities and stability of the active Au NPs essentially rely on their surface functionalization. Thus, appropriately coated Au NPs as fluorescent or photo-thermal active probes, with capabilities of passing cellular membranes, escaping the endosome and subcellular targeting features are of broad interest for advancing super-resolution bio-imaging applications.

We present a versatile polypeptide copolymer approach to efficiently stabilize ultra-small, NIR-Au NPs below 2 nm as well

[a]*Institute of Organic Chemistry III, Ulm University, Albert-Einstein-Allee 11, D-89081 Ulm, Germany. E-mail: Tanja.Weil@uni-ulm.de*
[b]*Max-Planck-Institute for Polymer Research, Ackermannweg 10, 55128 Mainz, Germany. E-mail: weil@mpip-mainz.mpg.de*
[c]*École Polytechnique Fédérale de Lausanne, Laboratoire d'Optique Biomédicale, Ch-1015 Lausanne, Switzerland*
[d]*Central Facility of Electron Microscopy, University of Ulm, Albert-Einstein-Allee 11, D-89081 Ulm, Germany*
[e]*Hepia, University of Applied Sciences of Western Switzerland (HES-SO), 4 rue de la Prairie, Ch-1202 Genève, Switzerland*
†Electronic supplementary information (ESI) available. See DOI: 10.1039/c6bm00951d

as larger Au NPs suitable for OCM imaging of subcellular compartments.[22,23] Such copolymers were obtained from native protein precursors as described previously.[24–26]

Such biopolymers offer defined contour lengths and precisely known monomer sequences of natural diversity, excellent biocompatibility[24,27] and various functional groups suitable for the attachment of the desired functionalities, *i.e.* drug molecules and cell-targeting groups.[28] These copolymers can be characterized by mass spectrometry to ensure the presence of all newly introduced functionalities along the polymer backbone as well as at the Au NP surface after coating. Herein, functional Au NPs are prepared in the presence of the multifunctional polypeptide copolymer, which imparts excellent water solubility, biocompatibility and stability under various physiological conditions as well as enhanced cellular uptake, endosomal release and subcellular targeting of mitochondria. Copolymer-coated Au NPs allow simultaneous tracking of mitochondria with either ultra-small NIR-Au NPs suitable for high resolution STED imaging as well as larger Au NPs for photo-thermal imaging with OCM, which underlines their significance as organelle specific probes in different microscopic techniques for studying dynamics inside living cells. Such a multifunctional, biocompatible polymer platform provides great potential for designing traceable nanotransporters for delivering cargos, such as drugs, to these cellular compartments.

For the synthesis of the known multifunctional peptide–polymer biopolymer 4 [24] shown in Scheme 1, the blood plasma protein human serum albumin (HSA, 1) serves as precursor, whose available carboxylic acid groups are converted into primary amino groups to yield polycationic HSA (cHSA, 2).[24] cHSA offers an increased number of reactive sites for all subsequent chemical modifications as well as enhanced cellular surface attachment and cellular uptake based on electrostatic interactions.[26] cHSA is denatured to yield dcHSA (3) and the newly formed thiol groups (35 thiols available in total) are reacted with polyethylene oxide (PEO) side chains that impart water-solubility and reduce nonspecific interactions.[24,29] The

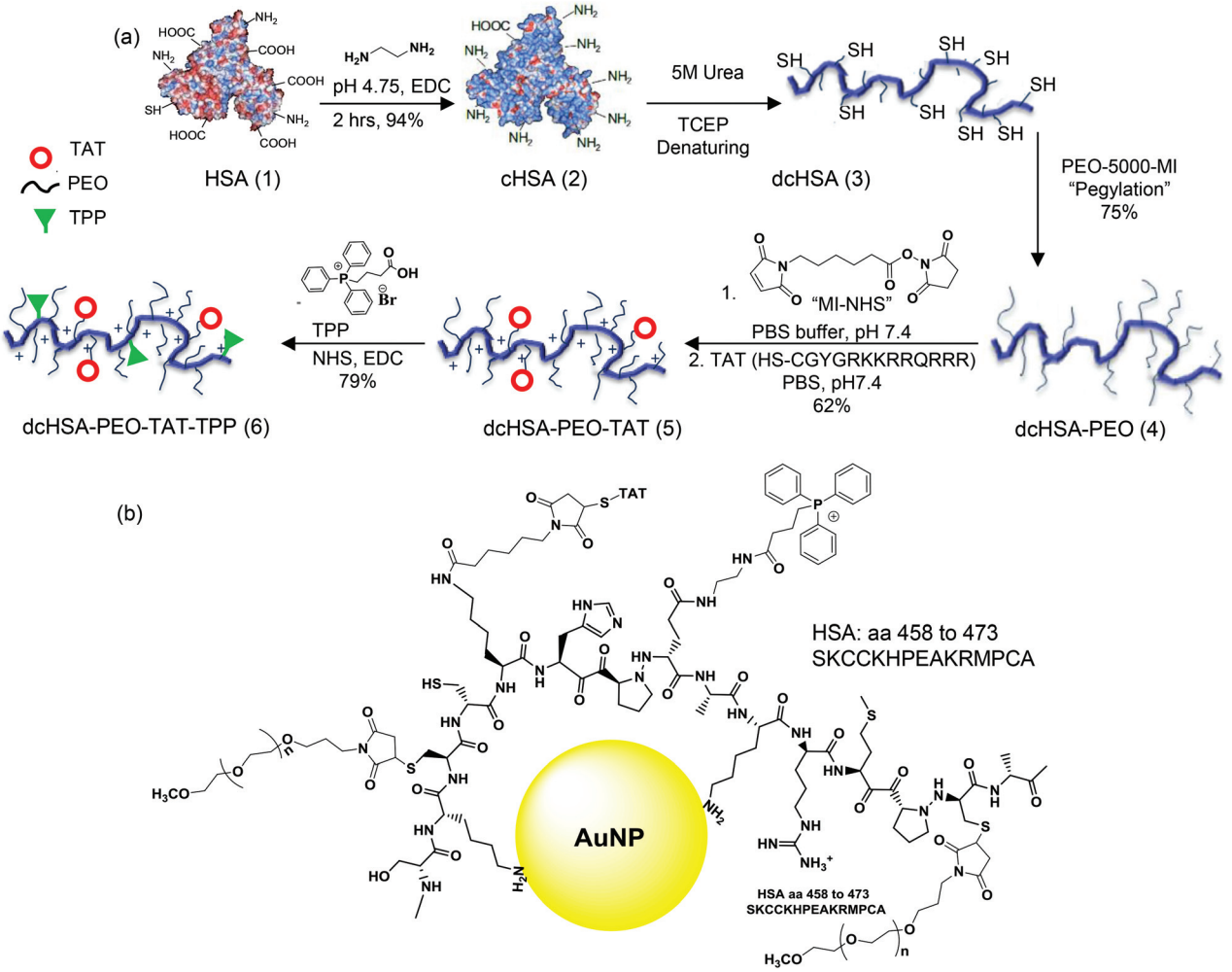

Scheme 1 (a) Synthesis scheme of dcHSA-PEO-TAT-TPP biopolymer (6) derived from globular HSA protein (1) after the attachment of ethylenediamine groups (2, cationization, cHSA), protein denaturing (3, dcHSA) and the attachment of PEO (4), TAT (5) and TPP (6). (b) Schematic illustration of polypeptide coated Au NP with any of the respective functionalities at distinct amino acid residues of the polypeptide chain.

resultant dcHSA-PEO hybrid (4) provides an optimal scaffold for further modifications. To improve cellular uptake into mammalian cells and enhance endosomal escape, several copies of the TAT peptide have been added. *N*-Hydroxy-succinimide activated maleimide (MI-NHS) is first reacted with biopolymer (4) in PBS buffer at pH 7.4. Subsequently, the terminal thiol of the cysteine (Cys) residue of TAT (SH-Cys-Gly-Tyr-Gly-Arg-Lys-Lys-Arg-Arg-Gln-Arg-Arg-Arg) is reacted with the newly introduced maleimide group of 4 to yield dcHSA-PEO-TAT (5). Lipophilic cations, such as triphenyl-phosphonium cation (TPP) are widely known for their selective accumulation in mitochondria.[28] The attachment of hydrophobic triphenyl phosphonium cations is carried out following the EDC-NHS ester coupling reaction (Scheme S3†) to yield the dcHSA-PEO-TAT-TPP (6) bioconjugate.

All of the above conjugates are characterized through Gel permeation chromatography, zeta-potential measurement, dynamic light scattering (DLS), and FTIR spectroscopy. Clear indication of the relative increase in molecular weights, zeta-potentials, and average sizes verifies successful synthesis of 6 (Fig. S1–S3†). In addition, the presence of a phosphorous peak in high resolution X-ray photoelectron spectroscopy (XPS) data, after TPP attachment (Fig. S1(b)†), provides further confirmation.

Ultra-small Au NPs are synthesized in aqueous solutions with 6 following a "one-pot", protein templated, green approach with slight modifications from the literature.[30] Au-salt (chloroauric acid, $HAuCl_4$) is mixed with 6 at 37 °C under slightly basic conditions as reported in detail in the ESI.† The final solution has pale yellow colour, which is a clear indication for the formation of dimensionally very small Au NPs. The Au NPs are washed with Milli-Q water to remove excess base and further purified using a Vivaspin 20 (MWCO30k) centrifugal concentrator and subjected to characterization by UV-Vis absorption and fluorescence spectroscopy as depicted in Fig. 1(a). No observable surface plasmon resonance features are present in the UV-Vis spectrum. The maximum emission occurred in the NIR region at 680 nm upon excitation at 405 nm due to the discrete and size-tunable electronic transition based on the spatial confinement of the free electrons in Au NPs. The quantum yield (QY) of these fluorescent Au NPs has been determined as ~6.1% with freshly prepared tris (2,2′-bipyridyl) ruthenium hexahydrate(II) as reference. This value is comparable to the highest reported QY of Au NPs in the literature.[30] Inset in Fig. 1(a) is the digital image of the biopolymer capped Au NP solution under room light and 365 nm UV light illumination revealing a strong emission originating from the efficient surface passivation of the Au NPs by the polypeptide backbone. Most likely, free primary amine groups present in 6 facilitated the reduction of the Au salt to form small clusters over time. From the time lapse study, presented in Fig. 1(b), slow formation of small Au NPs is clearly visible. Au NPs with maximum emission intensities are obtained after 24 h of continuous stirring. Beyond 24 h, precipitation of the biopolymer and aggregation of the particles occurred. Slow particle formation seems to be critical to achieve Au NPs with high QYs. In a control experiment, a strong reducing agent such as $NaBH_4$ has been applied that produced small clusters within minutes. However, we have observed very low QYs and broad size distributions of the particles. The Au NPs are purified through ultracentrifugation to remove excess quantities of $NaBH_4$ and characterized *via* UV-Vis and fluorescence spectroscopy (Fig. S5†).

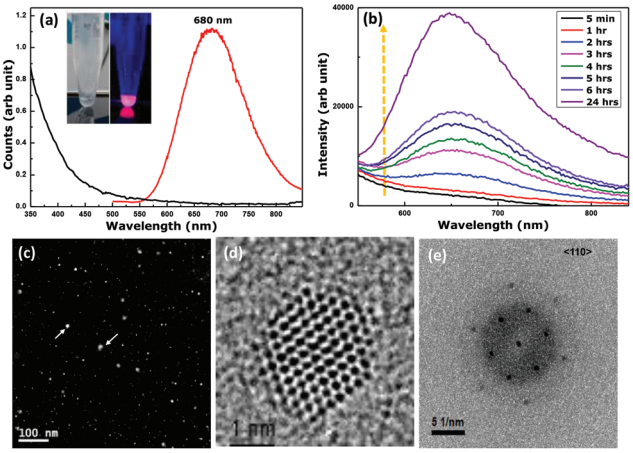

Fig. 1 (a) Typical absorbance and emission spectra of Au NPs. No plasmon resonance is observed in the absorbance spectra indicating the formation of small nanoparticles that emit at 680 nm. Inset contains the digital image of highly fluorescent Au NPs with and without UV light illumination. (b) Time evolution of the fluorescence spectra for the reaction solutions are depicted where each sample was excited at 365 nm. (c) HAADF-STEM image of dcHSA-PEO-TAT-TPP coated Au nanoparticles showing single crystals as tiny white spots. The larger spots belong to crystal agglomerations (white arrow). (d–e) Aberration-corrected HRTEM image and corresponding fast Fourier transform (FFT) of a typical Au-nanocrystal in <110> orientation. The 111-reflex showed *d*-spacing of 2.36 Å.

To image the Au nanoparticles, transmission electron microscopy (TEM) was carried out using a FEI Titan 80-300 operated at 300 kV. The solution of nanoparticles was drop-coated on standard thin carbon film on Cu grids. A wider-view high-angle annular dark-field scanning TEM (HAADF-STEM) image (Fig. 1c) and a representative aberration-corrected high-resolution (AC-HR) TEM image (Fig. 1d) clearly indicate that as-synthesized Au NPs were well dispersed. The average size has been determined to be 2.0 ± 0.5 nm. These small sizes nicely correspond to the UV-Vis spectra, where no observable plasmonic peaks are present. The protein structure around the particles is destroyed rapidly due to damage during the imaging process. Moreover, the amorphous carbon film of the TEM grids spoils any weak contrast features. An energy dispersive X-Ray (EDX) spectrum (Fig. S4b†) displays the presence of Au as well as a very high nitrogen content, which can be attributed to the presence of the polypeptide chain containing large numbers of amine groups.

For bio-imaging applications, the colloidal stability of the biopolymer-Au structures in the presence of high salt concentrations as well as proteases is essential. For this purpose, the emission profiles in the presence of 30% (v/v) (a) 10 mM phos-

phate buffer and 2% glucose, (b) 1 M NaCl, (c) pH 3.9, (d) pH 10 and (e) the protease trypsin are examined (Fig. S6†). After 24 h of incubation, the emission properties of the biopolymer-Au constructs remain unchanged indicating high colloidal stabilities under various physiological conditions suitable for *in vitro* applications.

The cellular uptake efficiency and intracellular localization of Au NPs coated with dcHSA-PEO-TAT-TPP (6) has been evaluated by laser scanning confocal microscopy. Typically, HeLa cells are incubated with the fluorescent biopolymer-coated AuNPs for about 18 h before image acquisition. The NIR-emitting biopolymer-Au NPs are mainly located in the cytosol, outside the nuclear region (Fig. 2 and 3). Staining the mitochondria with a mito-tracker dye, we observe clear co-localization as depicted in Fig. 3, where the Pearson's coefficient is calculated to be 0.89, indicating agreeable colocalization of the dcHSA-PEO-TAT-TPP-Au NPs (6) with mitochondria. The red emission is related to mitotracker Red-stained mitochondria, while the green colour corresponds to the fluorescence signal of the Au NPs excited at 405 nm. The appearance of a yellow colour from the merged red and green channels indicates the co-localization of the Au NPs in the mitochondria cell compartment.

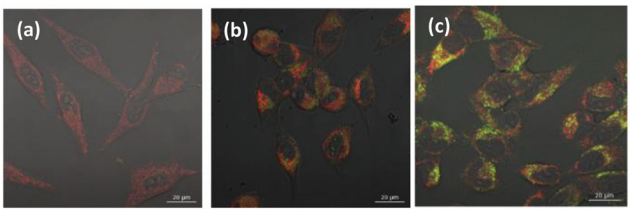

Fig. 2 (a–c) Confocal microscopy images of HeLa cells incubated with Au NPs coated with (a) dcHSA-PEO-TPP, (b) dHSA-PEO-TAT-TPP (6) and (c) dcHSA-PEO-TAT (5) after 18 h incubation (λ_{ex} = 405 nm). Overlay images using simultaneous scanning of Au NPs (green spots) and MitoTrackerR Red CM-H2XRos (Invitrogen) (red spots).

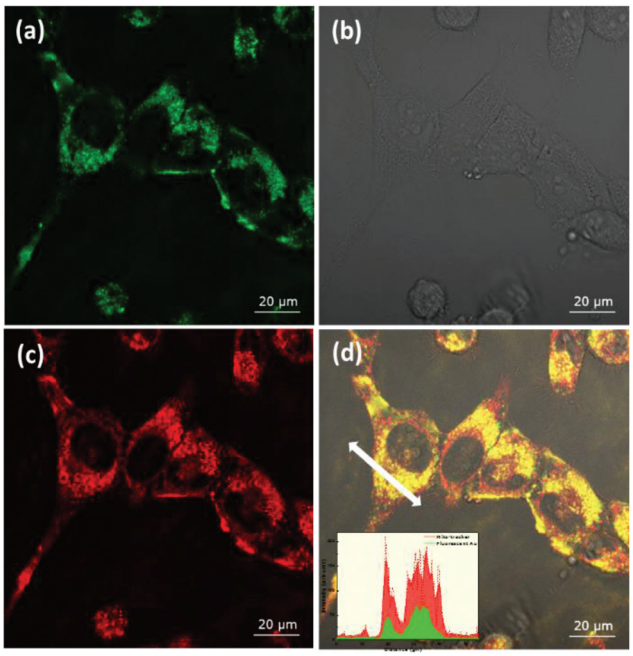

Fig. 3 (a–d) Confocal microscopy image of HeLa cells incubated with dcHSA-PEO-TAT-TPP-Au NPs, where (a) shows the emission from small Au NP clusters (λ_{ex} = 405 nm), (b) cell under white light, (c) fluorescence from mito-tracker and (d) overlay of all 3 images. Inset in (d), shows the line scanning profile of fluorescent intensity (along the white arrow; green colour from fluorescent Au and red colour from mito-tracker).

Control experiments with Au NPs coated with structurally similar biopolymers that have neither been cationized (HSA instead of cHSA, Fig. 2b) nor possess TAT peptides (Fig. 2a) or TPP groups exhibit no or only poor cellular uptake and endosomal release or mitochondria targeting capabilities, respectively (Fig. 2c and S7–S9†). TAT has been reported previously to serve as mito-tracker[31] and therefore, we have synthesized and investigated Au NPs coated with dcHSA-PEO-TAT (5) that did not contain TPP. Au NPs coated with (5) without TPP clearly show very little colocalization with mitochondria (Fig. 2c and S10†) and therefore, the presence of all three functionalities, *i.e.* multiple primary amino groups after cationization of HSA and several TAT peptides are both crucial for achieving enhanced cellular uptake and endosomal release, whereas the TPP is essential to direct the Au NPs to the mitochondria of the cells (Fig. 3).

Next, we investigated the capacity of 6 for stabilizing larger Au NPs and for their trafficking to a desired intracellular target. Larger Au NPs are prepared *in situ*, when $HAuCl_4$ is reduced by $NaBH_4$ in presence of 6. Fig. S11† and shows relatively uniform and well dispersed Au NPs with average sizes of 4 ± 1.3 nm. Due to their larger size, these particles showed plasmonic behaviour, which could be exploited for photothermal optical lock-in OCM (poli-OCM) imaging. Fig. 4(a–c) represent the corresponding poli-OCM images of the cells after incubation of 6 and 4 nm Au NPs with HeLa cells for 18 h. Green colour results from the photo-thermal signal of the Au NPs and the red colour is related to mitotracker red-stained mitochondria. The appearance of yellow colour indicates colocalization of large Au NPs and mitochondria. A reconstructed 3D image is demonstrated in Fig. 4(d), where the yellow spots resemble the presence of mitochondria inside living cells. Noteworthy, both small and large Au NPs did not impose any cellular toxicity under the imaging conditions applied herein (Fig. S6(f and g)†).

In addition, we have optimized the conditions for the photothermal scattering signal in OCM by increasing the concentration of AuNPs inside the cells. Fig. 4(f) shows the mean intensity of the poli-OCM signal for different concentrations of AuNPs. The photothermal signal has a linear relationship with the absorbance cross section of the particle (see eqn (S1)†). Therefore, increasing the concentration of Au NPs should proportionally increase the number of absorbers within the excitation volume of the photothermal heating beam. However, from Fig. 4(e), we can conclude that the photothermal signal does not follow the linear relationship with increasing concentrations of AuNPs. We believe that higher concentrations could

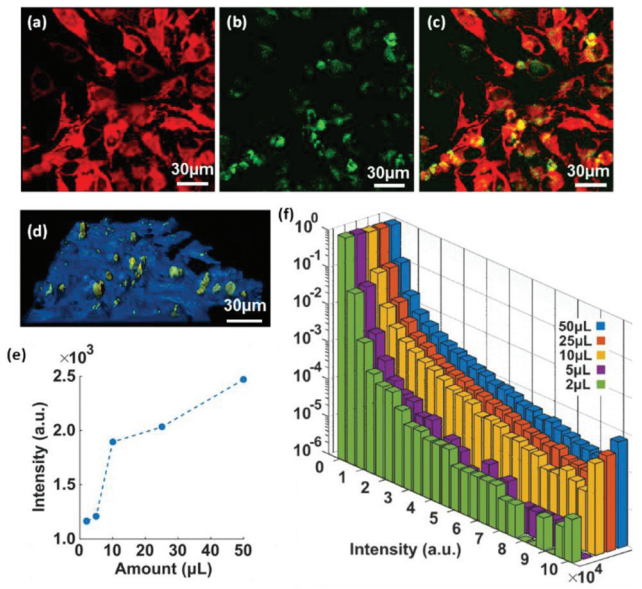

Fig. 4 Optical coherence microscopy (OCM) image of HeLa cells incubated with 4 nm sized dcHSA-PEO-TAT-TPP-Au NPs, where (a) depicts the fluorescence from mito-tracker (b) the photo-thermal signal from large Au NPs, and (c) the overlay of both images. The scale bar is 20 micrometres. (d) Constructed 3D images of the cells where yellow areas indicate the presence of mitochondria. (e) Average poli-OCM signal intensity acquired from cell cultures incubated with different concentration of AuNPs. (f) Normalized histogram of poli-OCM signal intensity for increasing the AuNP concentrations.

increase the probability of aggregation and consequently the interactions between neighboring Au NPs, which would result in more intense signals (Fig. S13†). Furthermore, we present histograms of the poli-OCM signal in Fig. 4(f) for different AuNP concentrations that illustrate a shift to higher scattering intensities as the Au NP concentration is increased.

In summary, we have reported a versatile protein-derived polypeptide platform, which even allows attaching multiple copies of up to four different kinds of functionalities: long PEO chains improved solubility and stability, whereas the primary amines facilitated interactions with cellular membranes as well as further post-modifications. TAT and TPP were selected to impart cellular uptake and intracellular release, whereas TPP facilitated subcellular targeting. This high degree of side chain functionalization is due to the availability of various reactive groups distributed over the entire polypeptide backbone and even after functionalization, sufficient numbers of polar groups remained that could complex gold cations to initiate the nucleation processes. We could demonstrate the synthesis of ultra-small (≈2 nm) and fluorescent NIR-Au NPs that reveal biocompatibility and high stability under physiological conditions and they remained aggregation-free in water under ambient conditions for several months. This method has also been adapted to achieve larger, 4 nm sized Au NPs that are particularly useful for poli-OCM imaging *e.g.* to study mitochondria trafficking and dynamics inside living cells based on their remarkable mitochondria targeting capabilities.[32] The biopolymer synthesis and Au NP coating approach reported herein yields multifunctional Au NPs providing access to different imaging techniques. In contrast to Au NP surface coating by various small molecule ligands, the availability of such multifunctional polymers ensures the presence of all functionalities at the NP surface after coating. The synthetic methodology reported herein could be easily adapted to different cell penetrating and subcellular targeting peptides. Therefore, multifunctional Au NPs reported herein represent a valuable tool for advanced live cell imaging with subcellular accuracy. Due to the potential of Au NPs in cancer therapy, the synthesis strategy could also be highly attractive for developing various smart diagnostic and therapeutic tools.

Acknowledgements

The authors declare no competing financial interest. The manuscript was written through contributions of all authors. All authors have given approval to the final version of the manuscript. The authors are grateful to the financial support of the German Research Foundation (DFG) under P3246029. Open Access funding provided by the Max Planck Society.

Notes and references

1 L. Rajendran, H.-J. Knölker and K. Simons, *Nat. Rev. Drug Discovery*, 2010, **9**, 29–42.
2 R. Gorelik, C. Yang, V. Kameswaran, R. Dominguez and T. Svitkina, *Mol. Biol. Cell*, 2011, **22**, 189–201.
3 J. J. Dumas, E. Merithew, E. Sudharshan, D. Rajamani, S. Hayes, D. Lawe, S. Corvera and D. G. Lambright, *Mol. Cell*, 2001, **8**, 947–958.
4 R. Luetterforst, E. Stang, N. Zorzi, A. Carozzi, M. Way and R. G. Parton, *J. Cell Biol.*, 1999, **145**, 1443–1459.
5 A. L. J. Marschall, A. Frenzel, T. Schirrmann, M. Schüngel and S. Dübel, *mAbs*, 2011, **3**, 3–16.
6 R. A. J. Smith, R. C. Hartley and M. P. Murphy, *J. Bioenerg. Biomembr.*, 2013, **45**, 165–173.
7 A. Deepthi and S. Raju, *J. Pharm. Sci. Res.*, 2013, **5**, 48–56.
8 S. Biswas and V. P. Torchilin, *Adv. Drug Delivery Rev.*, 2014, **66**, 26–41.
9 J. W. Kang, P. T. C. So, R. R. Dasari and D.-K. Lim, *Nano Lett.*, 2015, **15**, 1766–1772.
10 S. Cox, *Dev. Biol.*, 2014, **401**, 175–181.
11 R. A. Leitgeb, M. Villiger, A. H. Bachmann, L. Steinmann and T. Lasser, *Opt. Lett.*, 2006, **31**, 2450–2452.
12 A. Fercher, W. Drexler, C. Hitzenberger and T. Lasser, *Rep. Prog. Phys.*, 2003, **66**, 239–303.
13 C. Pache, N. L. Bocchio, A. Bouwens, M. Villiger, C. Berclaz, J. Goulley, M. I. Gibson, C. Santschi and T. Lasser, *Opt. Express*, 2012, **20**, 21385.
14 A. Parodi, C. Corbo, A. Cevenini, R. Molinaro, R. Palomba, L. Pandolfi, M. Agostini, F. Salvatore and E. Tasciotti, *Nanomedicine*, 2015, **10**, 1923–1940.

15 J. Zheng, C. Zhang and R. M. Dickson, *Phys. Rev. Lett.*, 2004, **93**, 5–8.
16 C. A. J. Lin, C. H. Lee, J. T. Hsieh, H. H. Wang, J. K. Li, J. L. Shen, W. H. Chan, H. I. Yeh and W. H. Chang, *J. Med. Biol. Eng.*, 2009, **29**, 276–283.
17 G. Wang, T. Huang, R. W. Murray, L. Menard and R. G. Nuzzo, *J. Am. Chem. Soc.*, 2005, **127**, 812–813.
18 X. Tu, W. Chen and X. Guo, *Nanotechnology*, 2011, **22**, 95701.
19 X. Le Guével, B. Hötzer, G. Jung and M. Schneider, *J. Mater. Chem.*, 2011, **21**, 2974.
20 J. Zheng, C. Zhou, M. Yu and J. Liu, *Nanoscale*, 2012, **4**, 4073.
21 J. Liu, P. N. Duchesne, M. Yu, X. Jiang, X. Ning, R. D. Vinluan, P. Zhang and J. Zheng, *Angew. Chem., Int. Ed.*, 2016, **55**, 8894–8898.
22 M. Kodiha, Y. M. Wang, E. Hutter, D. Maysinger and U. Stochaj, *Theranostics*, 2015, **5**, 357–370.
23 O. S. Adeyemi and F. A. Sulaiman, *J. Biomed. Res.*, 2015, **29**, 145–149.
24 Y. Wu, G. Pramanik, K. Eisele and T. Weil, *Biomacromolecules*, 2012, **13**, 1890–1898.
25 Y. Wu, S. Chakrabortty, R. A. Gropeanu, J. Wilhelmi, Y. Xu, K. S. Er, S. L. Kuan, K. Koynov, Y. Chan and T. Weil, *J. Am. Chem. Soc.*, 2010, **14**, 5012–5014.
26 Y. Wu, K. Eisele, M. Doroshenko, G. Algara-Siller, U. Kaiser, K. Koynov and T. Weil, *Small*, 2012, **8**, 3465–3475.
27 D. W. N. Yuen, Y. Wu, S. L. Kuan and T. Weil, *Acc. Chem. Res.*, 2014, **47**, 3471–3480.
28 S. V. Boddapati, P. Tongcharoensirikul, R. N. Hanson, G. G. M. D'Souza, V. P. Torchilin and V. Weissig, *J. Liposome Res.*, 2005, **15**, 49–58.
29 S. El-Andaloussi, P. Järver, H. J. Johansson and U. Langel, *Biochem. J.*, 2007, **407**, 285–292.
30 J. Xie, Y. Zheng and J. Y. Ying, *J. Am. Chem. Soc.*, 2009, **131**, 888–889.
31 V. Del Gaizo and R. M. Payne, *Mol. Ther.*, 2003, **7**, 720–730.
32 M. Sison, S. Chakrabortty, J. Extermann, A. Nahas, J. P. Marchand, A. Lopez, T. Weil and T. Lasser, *Sci. Rep.*, 2017, **7**, 43275, DOI: 10.1038/srep43275.